Published in final edited form as:

Pediatr Res. 2017 July ; 82(1): 122–132. doi:10.1038/pr.2017.78.

Hepatic MDR3 expression impacts lipid homeostasis and susceptibility to inflammatory bile duct obstruction in neonates

Alexandra N. Carey[1,♯], **Wujuan Zhang**[2,♯], **Kenneth D.R. Setchell**[2,6], **Julia E. Simmons**[1], **Tiffany Shi**[1], **Celine S. Lages**[1], **Mary Mullen**[1], **Kaitlin Carroll**[3], **Rebekah Karns**[4], **Kazuhiko Bessho**[1], **Rachel Sheridan**[2], **Xueheng Zhao**[2], **Susanne N. Weber**[5], and **Alexander G. Miethke**[1,6,*]

[1]Division of Pediatric Gastroenterology, Hepatology, and Nutrition, Cincinnati Children's Hospital Medical Center (CCHMC), Cincinnati, Ohio

[2]Division of Pathology and Laboratory Medicine, CCHMC, Cincinnati, Ohio

[3]Division of Immunobiology, CCHMC, Ohio

[4]Division of Biomedical Informatics, CCHMC, Ohio

[5]Universitaetsklinikum des Saarlands, Homburg, Germany

[6]Department of Pediatrics, University of Cincinnati College of Medicine, Cincinnati, Ohio

Abstract

Background—Heterozygous mutations in the gene *ABCB4*, encoding the phospholipid floppase MDR3 (Mdr2 in mice), are associated with various chronic liver diseases. Here, we hypothesize that reduced *ABCB4* expression predisposes to extrahepatic biliary atresia (EHBA).

Methods—Livers from neonatal wildtype (wt) and heterozygous Mdr2-deficient mice were subjected to mass-spectrometry based lipidomics and RNAseq studies. Following postnatal infection with rhesus rotavirus (RRV), liver immune responses and EHBA phenotype were assessed. Hepatic microarray data from 40 infants with EHBA were mined for expression levels of *ABCB4*.

Results—Phosphatidylcholine (PC) and phosphatidylethanolamine (PE) were increased while the PC/PE ratio was decreased in neonatal *Mdr2*$^{+/-}$ compared with wt mice. Following RRV challenge, hepatic expression of IFNγ and infiltration with CD8+ and NK+ lymphocytes were increased in *Mdr2*$^{+/-}$ mice. Plasma total bilirubin levels and prevalence of complete ductal obstruction were higher in these mice. In infants with EHBA, hepatic gene expression of *ABCB4*

*Corresponding author: Alexander G Miethke, MD Assistant Professor of Pediatrics Pediatric Gastroenterology, Hepatology, and Nutrition MLC 2010 Cincinnati Children's Hospital Medical Center 3333 Burnet Avenue Cincinnati, OH 45229 Phone: 513.636.8948, Fax: 513.636.5581, alexander.miethke@cchmc.org.

♯Authors contributed equally to the manuscript

Disclosure: The authors disclose no conflicts of interest.

Category of Study: Basic science

was downregulated in those with an inflammatory compared with a fibrosing molecular phenotype.

Conclusions—Decreased expression of *ABCB4* causes dysregulation in (phospho)lipid homeostasis, and predisposes to aberrant pro-inflammatory lymphocyte responses and an aggravated phenotype of EHBA in neonatal mice. Downregulated *ABCB4* is associated with an inflammatory transcriptome signature in infants with EHBA.

Introduction

The main constituents of bile, including bile acids (BA), phospholipids (PL; mainly phosphatidylcholines) and cholesterol, are actively excreted from hepatocytes into the bile across the canalicular membrane by the proteins BSEP (encoded by the gene *ABCB11*), MDR3 (*ABCB4*) and ABCG5/8 (*ABCG5/8)* respectively, all members of the ABC transporter family. Impaired expression of these transporters results in well recognized clinical syndromes of chronic cholestasis, typically with onset in infancy. The most severe phenotypes result from bi-allelic mutations in the respective genes, for instance in progressive familial intrahepatic cholestasis (PFIC) type 2 due to mutations in *ABCB11*, a syndrome of chronic cholestasis associated with low or normal serum gamma-glutamyltransferase (GGT) activity and an absence or low level of bile salts in bile, whereas dual mutations in *ABCB4* cause a fibrosing cholangiopathy with high serum GGT levels and absence of biliary PL. MDR3-disease is associated with a variety of liver disease phenotypes, ranging from neonatal onset of cholestatic jaundice, commonly referred to as PFIC type 3, to low phospholipid intrahepatic gallstones, and biliary fibrosis with characteristic radiographic and histologic features (1–3). Histologically it is characterized by a cholangiopathy with bile duct epithelial injury and ductal proliferation, portal inflammation, and variable stage of fibrosis. Severe reduction of biliary phospholipids in MDR3 deficiency in humans, or of the orthologue Mdr2 in mice, was shown to predispose to biliary microcrystal formation, cholangiocyte injury, and hepatocellular carcinoma (4).

A recent population based genome sequencing study in Iceland detected four variants in the gene *ABCB4* that confer risk for the development of gallstones, intrahepatic cholestasis of pregnancy (ICP), HCC and cholangiocarcinoma, and cirrhosis (5), thus rendering *ABCB4* the gene with perhaps the most significant contributions to inherited liver disease, similar to that of the *PNPLA3*. Importantly, there has been increasing evidence for rare *ABCB4* variants causing liver disease in both autosomal dominant as well as recessive inheritance patterns. For instance, heterozygous missense mutations, which impair trafficking of MDR3, were associated with ICP(6). Heterozygous mutations in *ABCB4* have also been linked to idiopathic fibrosing cholestatic liver disease in adults (7), chronic cholestatic biochemistry profile and family history of liver disease (8), and early onset of primary sclerosing cholangitis (8). Recently, heterozygous variants in *ABCB4* were also detected in a cohort of 9 children with idiopathic chronic cholestasis with first onset of symptoms between 2 months and 11 years of age (9). In five subjects, haploinsufficiency for *ABCB4* was associated with other liver diseases, including extrahepatic biliary atresia (EHBA). Coexistence of heterozygous variants in *ABCB4* and in functionally related genes like *ABCB11* and *ATP8B1* were found to be more frequent in children with idiopathic

cholestasis than in healthy controls (10). However, the mechanisms of how reduction in MDR3 expression due to heterozygous mutations modulates co-existing liver diseases are currently unknown.

Material and Methods

HUMAN STUDIES

Case report—The female patient was born small for gestational age at a Kenyan refugee camp (birth weight 1.5kg), noted to be jaundiced at 7 months of age. She was diagnosed with PFIC3/MDR3 disease based on clinical genetic testing which revealed two non-synonymous variants in *ABCB4* (c.2363G>A [pR788Q] and c.101C>T [pT34M]) interpreted as pathogenic and as variant of uncertain significance, respectively. She presented to our center at 13 months of age with serum biochemistries notable for significant cholestasis (conjugated bilirubin 13 mg/dL, alkaline phosphatase 700 IU/L, GGT 600IU/L, total serum bile acids 128 μmol/L), moderate hepatocellular injury (AST 400IU/L and ALT 200IU/L) and with coagulopathy (prothrombin time 19.5 sec). The patient developed ascites, variceal bleeding and ultimately underwent liver transplantation at 23 months of age. The explanted liver showed histomorphological features of MDR3 disease and EHBA.

Hepatic microarray studies—Relative *ABCB4* gene expression levels were analyzed in gene expression data originally obtained from hepatic microarray studies carried out on patients with EHBA at the time of diagnosis by intrahepatic cholangiograms (11). Detailed information on handling of liver biopsy samples, protocols for RNA labeling, chip hybridization and signals, internal controls, normalization procedures, and analysis of gene expression were deposited in Gene Expression Omnibus (GEO: GSE46995). The original study protocol conformed to the ethical guidelines of the 1975 Declaration of Helsinki and was approved by the human research committees of all participating institutions.

MURINE STUDIES

Abcb4 (Mdr2)$^{-/-}$ mice were originally derived in the FVB strain (12) and then backcrossed into the BALB/c strain in the laboratory of Dr. Lammert (Homburg/Germany) (4). In the established murine EHBA model, 1.5 ×10^6 ffu of rhesus rotavirus (RRV) is injected postnatally into BALB/c mice leading to bile duct obstruction(13). As a way to attenuate the EHBA phenotype, a lower dose of 0.5×10^6 ffu of RRV was injected intraperitoneally (i.p.) at day of life (DOL) 2. All mice were bred in house and kept in conventional conditions. All protocols were approved by the Animal Care and Use Committee of the Cincinnati Children's Research Foundation.

Phenotype of EHBA

The EHBA phenotype was assessed on day 8 post RRV challenge. Plasma total bilirubin concentration was measured using a colorimetric assay (Pierce Chemical Co., Rockford, IL). Zinc-fixed, paraffin-embedded extrahepatic bile ducts were sectioned and stained with H&E and patency was assessed on longitudinal sections by investigators blinded to the group assignment (ANC, AGM), as previously performed in studies on experimental EHBA (14).

iNOS Immunohistochemistry

5μm zinc-fixed mouse liver sections were subjected to antigen retrieval consisting of heat at high pressure for 15 minutes in 1M Sodium Citrate buffer, pH 6.0. Primary antibody against iNOS (rabbit; Abcam: Ab15323, Cambridge, UK**)** was diluted at 1:100 with blocking solution and incubated at 4°C overnight. Biotin-SP-conjugated Goat anti-rabbit (Jackson ImmunoResearch: 111-065-003; West Grove, PA) was applied at 1:1000 dilution and incubated for 2 hours at room temperature.

Protein blot analysis

Crude protein extracts from livers of neonatal mice were prepared by sonication on ice in RIPA Buffer. Lysates were centrifuged for 20 min, 14,000 rpm at 4°C, and the supernatants were used for SDS-PAGE on a 4–12% acrylamide Bis-Tris gel (Invitrogen, Carlsbad, CA) followed by transfer to a nitrocellulose membrane. Immunoblotting was performed with anti-MDR3 antibody (Kamiya Biomedical Co., Tukwila, WA) or anti-actin antibody (Santa Cruz Biotechnology, Santa Cruz, CA) diluted 1:1000 in 2.5% BSA blocking buffer followed by washes and incubation with a secondary antibody conjugated to horseradish peroxidase at 1:2000 dilution. Blots were developed with Super Signal West Pico (Thermo Scientific, Florence, KY). The molecular weights of ABCB4-encoded membrane-bound P-glycoprotein and of actin are 140 and 43 kDa, respectively.

Hepatic Mononuclear Cell (MNC) isolation, flow cytometric analysis

Mice were euthanized and perfused with 1% collagenase through the portal vein. Hepatic MNC were isolated as previously reported by our group (15). Following red cell lysis and washes, single cell suspensions were stained with PerCP-, PE-, APC, FITC and conjugated antibodies against CD3, CD8, NK, and CD4, respectively, and cell counts were acquired on an Accuri flow cytometer (BD Biosciences, Franklin Lakes, NJ). Flow cytometric data were compensated and analyzed using FlowJo Tree software (FlowJo LLC, Ashland, OR).

Quantitative PCR

Multiplex qPCR using the TaqMan Mouse Immune Array (Applied Biosystems) with genes encoding 88 cytokines and chemokines and 8 house-keeping genes and candidate SYBR green qPCR were performed as reported by our group before (16).

RNAseq

For RNAseq studies, total RNA was isolated from snap frozen samples from lobe 2 of livers from 10-day-old mice born to *Mdr2*$^{+/-}$ parental mice, kept as littermates until time of tissue harvest. RNA-seq libraries were prepared with the Illumina TruSeq RNA preparation kit and sequenced on the Illumina Hi-Seq 2000, as previously described (17). Differentially expressed genes with a fold change of >= 2.0 and $p<0.05$ between *Mdr2* $^{+/-}$ and +/+ neonatal mice were submitted to pathway enrichment analysis with ToppFun application from the ToppGene Suite, which uses unbiased methods to assess pathway enrichment (18). Raw and normalized data are accessible through NCBI's Gene Expression Omnibus (GEO accession number GSE78514).

Global lipidomic and targeted phospholipid analysis by liquid chromatography- mass spectrometry (LC-MS)—Liver tissue (lobe 1) was obtained from 10-day-old mice and subjected to exhaustive solvent extraction for lipids. Global lipidomics analysis was performed on a Xevo G2-S quadrupole time-of-flight (Q-TOF) mass spectrometer (MS) interfaced with an Acquity ultra-high performance liquid chromatography (UPLC) system (Waters, Milford, MA) operated in electrospray ionization mode. An Acquity CSH C18 UPLC column was used to chromatographically separate components over 20 minute gradient elution. Compounds were ionized with electrospray and positive and negative ions acquired over the mass range 50-1200 Daltons with high resolution. Deconvolution, peak alignment, and preliminary normalization were conducted on raw metabolomics data with Progenesis QI (Waters). Each compound ion feature was annotated by elution time with *m/z*. Raw data were normalized by total compound ion intensity and with a global scalar derived from logarithm ratio of each sample to the reference. Accurate molecular mass (*m/z*) was used to search against HMDB and lipid MAPS database for putative identification.

Targeted Phosphatidylcholine (PC) and phosphatidylethanolamine (PE) analysis

Quantitative analysis of PC and PE was carried out using a Waters API triple quadrupole mass spectrometer interfaced with an Acquity UPLC system and operated in electrospray ionization mode with negative ion acquisition. PLs were extracted from liver tissue by the Folch procedure and quantified using PC and PE standards with multiple reactions monitoring function. Total PC and PE were calculated based on the summation of 13 major PC species and 20 major PE species detected in plasma or liver.

Statistical analysis

Statistical significance was determined by unpaired t- or Fisher exact tests with a significance set at $p<0.05$. Multivariate analysis, i.e. principal component analysis (PCA) for global lipidomics data was conducted in R environment for statistical programming. Compound ions acquired from both positive and negative modes from same sample were combined in the PCA. Normalized abundance (area of feature peak normalized by the total compound ion abundance from that sample) of each compound ion was used in the analysis.

Results

Reduced expression of the protein Mdr2 in neonatal *Mdr2*$^{+/-}$ compared with wild type (wt) mice was confirmed by immunoblotting (Figure 1a). In order to characterize the influence of Mdr2 expression on the hepatic microenvironment in neonatal mice we performed global lipidomic studies on liver samples. Principal component analysis of a total of 7281 combined positive and negative compound ions acquired by accurate mass measurement revealed that *Mdr2*$^{+/-}$ mice clustered more closely in their metabolic signature with homozygous knockout and both genotypes were largely segregated from wt mice (Figure 1b). Compounds significantly accumulated in the liver of *Mdr2*$^{+/-}$ mice included several PC and PE species, i.e. PC (36:4), PC(36:2), PE (36:4), and PE (44:10) with their identity confirmed either with available reference standards or using our in-house lipid database.

Meanwhile, the hepatic levels for several triglyceride (TAG) species, including TAG (48:4) and TAG (60:12) were decreased in *Mdr2*$^{+/-}$ compared with wt mice (Figure 1c and d)

Candidates from this global lipidomics analysis were confirmed by targeted mass-spectrometry based quantitative analysis of PLs which revealed that total PC concentration was significantly higher in liver and plasma in neonatal *Mdr2*$^{+/-}$ compared with wt mice (Figure 2a). The other predominant hepatic phospholipid class, PE, was also found to accumulate in *Mdr2*$^{+/-}$ compared with wt mice. Targeted quantitative analysis of both PC and PE validated the lipid data acquired in an unbiased fashion on the Q-TOF mass spectrometery platform (Figure 2b). Importantly, the ratio of PC/PE, which was previously shown to negatively correlate with liver injury and impaired regeneration (19), was decreased in *Mdr2*$^{+/-}$ compared with wt mice (molar ratio of PC/PE: 2.6 vs 1.9 in neonatal wt vs *Mdr2*$^{+/-}$, $p<0.05$). For individual PL species, we found significant increases for 18:2 lysophosphatidylcholines (LPC) and several diacyl phosphatidylcholines were increased in plasma and liver of neonatal *Mdr2*$^{+/-}$ mice (Figure 2c).

To further characterize effects of reduced Mdr2 expression on liver metabolic and immune function in these mice we performed RNAseq. Genes associated with cholesterol and lipid metabolism were primarily downregulated in neonatal *Mdr2*$^{+/-}$ mice, including expression of the phosphatidylcholine transfer protein *pctp* gene which may contribute to retention of PLs in livers from *Mdr2*$^{+/-}$ mice (Figure 3a/b). Interestingly, genes associated with immune function were also differentially regulated in *Mdr2*$^{+/-}$ compared with wt mice. For instance, genes involved in T lymphocyte polarization like *irf4* and *il12a* were up-regulated in *Mdr2*$^{+/-}$ mice, whereas hepatic mRNA for genes linked to co-stimulation control of T-lymphocytes like *icos* and *cd27* were reduced (Figure 3c). These findings of MS-based global lipidomic and RNAseq studies raise the biological possibility that diminished hepatic expression of mdr2 renders the hepatic microenvironment to amplify pro-inflammatory responses upon challenge with appropriate triggers.

To test this hypothesis, we challenged neonatal *Mdr2*$^{+/-}$ and wt mice with an attenuated dose of RRV. By day 8pRRV, the virus was not actively replicating in the livers from mice of both genotypes, as shown by qPCR for the RRV specific viral protein VP6 (Figure 4a) and for NSP3 (data not shown). In the conventional model of RRV-induced EHBA using a higher virus dose, hepatic expression of these viral proteins peaks at day 7pRRV and rapidly disappears thereafter (13). Following RRV infection, *Mdr2* mRNA expression was upregulated in wt and *Mdr2*$^{+/-}$ mice (Figure 4b). Using flow cytometry, we found increased infiltration of the liver with NK and CD8 lymphocytes in *Mdr2*$^{+/-}$ compared with wt littermates on d8pRRV (Figure 4c). Using multiplex-gene expression profiling we found upregulation (≥2-fold) of 16 pro-inflammatory genes including *cxcl*-10 and -11, inducible nitric oxide synthase (*inos*), and *sele*, encoding E-selectin, in RRV infected *Mdr2*+/− compared with wt mice for (Figure 4d). Candidate gene expression studies with SYBR green qPCR confirmed upregulation of the Th1 and Th2 cytokines interferon-gamma (ifnγ) and interleukin (*il-5*), respectively (Figure 4e). Both cytokines were previously recognized to be key drivers of neonatal bile duct obstruction (13, 20). The upregulation of *inos* in *Mdr2*$^{+/-}$ mice, whose role in murine EHBA is largely undefined, was corroborated by

immunohistochemical studies showing increased immunoreactivity against iNOS in inflammatory cells infiltrating the portal triads of livers from RRV infected (Figure 4f).

In order to ascertain whether aggravated hepatic inflammation and immune activation in RRV-infected *Mdr2*$^{+/-}$ mice influenced their EHBA phenotype, we determined plasma levels for total bilirubin, a circulating biomarker for biliary obstruction, and ductal patency by histomorphological analysis. Total bilirubin levels were significantly increased in RRV-infected *Mdr2*$^{+/-}$ compared with wt littermates (Figure 5a). Furthermore, complete inflammatory obstruction of the bile ducts was found in four times more animals with heterozygous loss of mdr2 compared with controls (Figure 5b).

To validate our findings in human samples, we surveyed the patients at our institution with the clinical diagnosis of MDR3 disease and found one subject with the dual diagnosis of MDR3-disease and EHBA. The liver explant of this 23-months-old female was remarkable for biliary cirrhosis (Figure 6Aa). In addition to changes typically seen in EHBA, for instance, absent gallbladder, complete obliteration of the extrahepatic bile ducts (Figure 6Ab) and bile duct proliferation with bile plugs (Figure 6Ad), features of MDR3 disease were also present, including intrahepatic gallstones (Figure 6Ac) and canalicular cholestasis (Figure 6Ae). This observation raised the possibility that in humans, similar to mice, reduced expression of the phospholipid floppase MDR3 predisposed to inflammatory hepatobiliary injury in the neonate. In order to further interrogate this hypothesis, we mined previously generated hepatic gene expression data from a cohort of 40 infants with EHBA (11). Based on the liver transcriptome, 36 of the subjects were assigned either an inflammatory (n=14) or a fibrosing molecular phenotype (n=22), using previously reported bioinformatics algorithms(21). In this cohort, mRNA expression for *ABCB4* was significantly lower in the 14 subjects with an inflammatory phenotype, characterized by upregulation of genes linked to activation of the pro-inflammatory transcription factors NFKB and NFAT, compared with the group with a fibrosing molecular phenotype, in which genes were abundantly expressed which encode proteins with binding sites for the profibrogenic transcription factors E2F and SP1 (Figure 6B).

Discussion

We have demonstrated that heterozygous loss of Mdr2 in neonatal mice leads to alterations in the hepatic and plasma lipid profiles, differential expression of genes involved in lipid metabolism and immune function, and predisposes to pro-inflammatory and enhanced polarized lymphocyte responses in the liver upon postnatal challenge with RRV. Mdr2$^{+/-}$ mice display an aggravated obstructive phenotype of EHBA compared with wt mice. In humans, decreased hepatic expression of *ABCB4* is associated with a molecular signature of inflammatory EHBA. Collectively, our data suggest that genetically determined alterations in hepatic PL metabolism may modulate hepatic immune function and confer susceptibility to inflammatory hepatobiliary injury in the neonate.

Systematic analysis of liver and plasma lipid and PL concentrations has not been performed in neonatal *Mdr2*$^{-/-}$ mice before. Previous studies in adult wt and *Mdr2*$^{-/-}$ mice demonstrated decreased concentration of serum PL in the knockout mice (22). Contrary to

the findings in adult mice, we found increased hepatic concentrations of PC and PE and lower levels of TAG in the neonatal *Mdr2*$^{+/-}$ and *Mdr2*$^{-/-}$ mice compared with wt animals.

The lipidomic profile of neonatal *Mdr2*$^{+/-}$ resembles more closely that of *Mdr2*$^{-/-}$ mice than wt mice. The reasons for this observation are unknown. We can only speculate that "physiologic cholestasis", caused by the immaturity of the neonatal liver in terms of bile acid and organic anion transporter development (23) and specifically expression of Mdr2 transcripts (24), further reduces Mdr2 mediated phospholipid floppase activity in neonates rendering the lipidomic profile in these mice more similar to homozygous knockout mice. The reduction of TAG in neonatal *Mdr2*$^{+/-}$ mice is noteworthy as loss in TAG storage capacity is critically linked to lipotoxicity and has been shown to exacerbate liver injury (25). Aiming at this metabolic pathway, high fat diet has been reported to increase hepatic TAG levels and to reverse liver injury in *Mdr2*$^{-/-}$ mice. Maternal intake of this diet was sufficient to inhibit development of sclerosing cholangitis and fibrosis in *Mdr2*$^{-/-}$ offspring (22).

Targeted quantitative analysis of liver tissue revealed increased total concentrations of PC and PE, and a decrease in the hepatic PC/PE ratio. These two classes of phospholipids are asymmetrically distributed in the plasma membrane: PC are mainly on the outer and PE are preferentially located on the inner leaflet, which makes the PC/PE ratio critical for plasma membrane permeability (26). Hepatic PC homeostasis is regulated by several processes, including biosynthesis from PE through the PE N-methyltransferase (pemt) pathway and efflux into the bile facilitated by mdr2. Mice deficient in pemt develop steatohepatitis and acute liver failure within 3 days of starting a choline-deficient diet (27) which is linked to a reduced PC/PE ratio and impaired membrane integrity. When this ratio is increased, liver injury can be prevented (19). Hepatic PC/PE has also been reported to be inversely correlated with the development of steatosis and inflammation in the progression of NAFLD (28). Consistent with the literature on disease progression in inflammatory liver diseases, our lipidomic data suggest that a decreased PC/PE ratio in *Mdr2*$^{+/-}$ mice may render these animals more susceptible to hepatobiliary injury during the neonatal period. To what degree our findings on lipid homeostasis in neonatal *Mdr2*$^{+/-}$ and *Mdr2*$^{-/-}$ mice in BALB/c background can be generalized to mice with impaired phospholipid floppase activity in other background strains requires further investigations. Progression of sclerosing cholangitis is reported to be accelerated in *Mdr2*$^{-/-}$ mice of BALB/c compared with FVB and C57BL6 backgrounds (29). Whether strain-specific differences in cholesterol and phospholipid absorption and lipoprotein formation, for which the FVB-strain is known to be a high HDL producer conferring resistance to atherosclerosis(30), also influence the liver disease phenotype is unknown. Strain-specific differences for kinetics of serum biochemistries correlating with cholestasis in *Mdr2*$^{-/-}$ mice were recently reported (31, 32).

We also found increased plasma concentrations for individual LPC and DPC species. LysoPCs have previously been linked to control of inflammatory pathways, especially during sepsis (33). Furthermore, LPC is known to induce IFNγ production by CD4+ lymphocytes (34), linking local tissue regulation of LPC and T cell activation with inflammatory tissue destruction, for instance in atherosclerosis. Additional help to T cell activation may be derived from LPC associated maturation of professional antigen

presenting cells and control of toll like receptors on monocytes(35). In our experimental setting, increased plasma and liver LPC/DPC concentrations in neonatal (non-infected) *Mdr2*$^{+/-}$ mice were associated with upregulation of hepatic expression of *IL12A* and *Irf4*, encoding proteins polarizing naïve T lymphocytes to a Th1 or Th2 phenotype, respectively. Following low dose RRV challenge, hepatic gene expression for Ifnγ and Il5 was higher in *Mdr2*$^{+/-}$ compared with infected wt mice. Both cytokine pathways have previously been linked to ductal obstruction in EHBA(36). Surges in expression of pro-inflammatory cytokines in *Mdr2*$^{+/-}$ mice correlated with liver infiltration with NK and CD8 lymphocyte responses, both found to be effector lymphocytes of neonatal bile duct obstruction (14, 37), and an aggravated EHBA phenotype. Several details on how the metabolic hepatic microenvironment predisposes to accelerated hepatobiliary injury in neonatal *Mdr2*$^{+/-}$ mice remain unknown. Although our experiments demonstrate that mRNA and protein expressions for mdr2 are both significantly reduced in neonatal, non-infected *Mdr2*$^{+/-}$ mice compared with wt mice, RRV infection causes upregulation of *Abcb4* mRNA expression in *Mdr2*$^{+/-}$ mice, resulting in similar expression levels of *Abcb4* in *Mdr2*$^{+/-}$ and wt mice following viral challenge. We speculate that the processes driving upregulation of pro-inflammatory gene expression and recruitment of effector lymphocytes to the liver begin early after viral challenge and are linked to the specific metabolic profiles observed in non-infected mice rather than to those developing following viral infection. Absence of viral replication at d8pRRV in both *Mdr2*$^{+/-}$ and wt mice suggests that hepatic Mdr2 reduction does not worsen the EHBA phenotype via promoting virus replication and direct virus cytopathic effects.

In validation studies using human tissue, we identified one African subject with a dual phenotype of EHBA and MDR3 disease harboring two non-synonymous variants in *ABCB4*. In addition, expression of *ABCB4* mRNA was decreased in livers from patients with EHBA and upregulation of pro-inflammatory genes compared with those of a fibrosing molecular phenotype. Comparison of liver transcriptomic data from studies in experimental RRV-induced EHBA with those in infants with EHBA is difficult given the plethora of environmental triggers implicated in the pathogenesis of human EHBA, including toxins and various viruses. Nevertheless, it is intriguing that *SELE*, encoding the endothelial vascular adhesion protein E-selectin, is upregulated in RRV-infected *Mdr2*$^{+/-}$ compared with wt mice and is also found to be preferentially expressed in infants with inflammatory EHBA and reduced *ABCB4* expression. Collectively, our data indicate that decreased hepatic expression of *ABCB4*, through either polymorphisms or inheritance of heterozygous deleterious mutations in this gene, may predispose infants to aggravated inflammatory responses in the liver conferring susceptibility to the development of EHBA. This conclusion is further supported by a recent pilot study demonstrating that the prevalence of the heterozygous non-synonymous variant p.A934T in *ABCB4* was higher in African American subjects and segregated with worse outcome, as evidenced by the need for early transplantation in a cohort of 195 children with EHBA (unpublished data) (38). None of the 97 subjects who survived with the native liver beyond the first 4 years of life carried this variant.

Here we provide mechanistic data linking reduced PL transporter expression with accumulation of biologically active lipid compounds (LPC) and polarization of immune responses, which if met by an environmental trigger may determine degree of liver

inflammation and disease phenotype. Whether in children with BA and pro-inflammatory phenotype, especially in those harboring non-synonymous mutations in ABCB4, inflammatory PLs are retained and the PC/PE ratio is decreased requires further investigations. In addition, future studies may aim at better understanding of the processes besides genetic predisposition which reduce expression of ABCB4/MDR3 in the neonatal liver, and whether pharmacological interventions targeting MDR3 expression or activity, i.e. through fibrates (39), have the potential to ameliorate the disease phenotype of EHBA.

Acknowledgments

We thank Dr. James Heubi (CCHMC) for the careful review of the manuscript and his thoughtful suggestions. We are grateful to Dr. Pranav Shivakumar for assistance in several of the experiments, and to Dr. Sujit Mohanty and Bryan Donnelly for providing primers and control cDNA for studies related to rotavirus replication.

Financial Support: The National Institute of Diabetes, Digestive and Kidney Diseases (NIDDK) grant DK095001 supported this study (to A.G.M.). The project was supported in part by PHS Grant P30 DK078392 (Pathology Core, Gene expression Core, Bioinformatics) of the Digestive Disease Research Core Center in Cincinnati, by the Childhood Liver Disease Research and Education Network (ChiLDReN) Grant: 5U01DK062453-12, National Institutes of Health Level VI Fellowship Award (to A.N.C.), by the American Liver Foundation Postdoctoral Research Fellowship Award (to A.N.C.), by the 2013 American Association for the Study of Liver Diseases Fellow Research Award, by National Institutes of Health Training Grant 5T32DK007727-18 (to A.N.C.) and by the National Center for Research Resources and the National Center for Advancing Translational Sciences, National Institutes of Health, through Grant 8 UL1 TR000077-04.

References

1. Davit-Spraul A, Gonzales E, Baussan C, Jacquemin E. The spectrum of liver diseases related to ABCB4 gene mutations: pathophysiology and clinical aspects. Semin Liver Dis. 2010; 30:134–146. [PubMed: 20422496]
2. Poupon R, Arrive L, Rosmorduc O. The cholangiographic features of severe forms of ABCB4/MDR3 deficiency-associated cholangiopathy in adults. Gastroenterol Clin Biol. 2010; 34:380–387. [PubMed: 20537830]
3. Vij M, Safwan M, Shanmugam NP, Rela M. Liver pathology in severe multidrug resistant 3 protein deficiency: a series of 10 pediatric cases. Ann Diagn Pathol. 2015; 19:277–282. [PubMed: 26117383]
4. Lammert F, Wang DQ, Hillebrandt S, et al. Spontaneous cholecysto- and hepatolithiasis in Mdr2−/− mice: a model for low phospholipid-associated cholelithiasis. Hepatology. 2004; 39:117–128. [PubMed: 14752830]
5. Gudbjartsson DF, Helgason H, Gudjonsson SA, et al. Large-scale whole-genome sequencing of the Icelandic population. Nat Genet. 2015; 47:435–444. [PubMed: 25807286]
6. Dixon PH, Weerasekera N, Linton KJ, et al. Heterozygous MDR3 missense mutation associated with intrahepatic cholestasis of pregnancy: evidence for a defect in protein trafficking. Hum Mol Genet. 2000; 9:1209–1217. [PubMed: 10767346]
7. Ziol M, Barbu V, Rosmorduc O, et al. ABCB4 heterozygous gene mutations associated with fibrosing cholestatic liver disease in adults. Gastroenterology. 2008; 135:131–141. [PubMed: 18482588]
8. Degiorgio D, Crosignani A, Colombo C, et al. ABCB4 mutations in adult patients with cholestatic liver disease: impact and phenotypic expression. J Gastroenterol. 2015
9. Gordo-Gilart R, Hierro L, Andueza S, et al. Heterozygous ABCB4 mutations in children with cholestatic liver disease. Liver Int. 2015
10. Goldschmidt ML, Mourya R, Connor J, et al. Increased frequency of double and triple heterozygous gene variants in children with intrahepatic cholestasis. Hepatol Res. 2015
11. Bessho K, Mourya R, Shivakumar P, et al. Gene expression signature for biliary atresia and a role for interleukin-8 in pathogenesis of experimental disease. Hepatology. 2014; 60:211–223. [PubMed: 24493287]

12. Smit JJ, Schinkel AH, Oude Elferink RP, Mol CA, et al. Homozygous disruption of the murine mdr2 P-glycoprotein gene leads to a complete absence of phospholipid from bile and to liver disease. Cell. 1993; 75:451–462. [PubMed: 8106172]
13. Shivakumar PCK, Sabla GE, Miethke A, et al. Obstruction of extrahepatic bile ducts by lymphocytes is regulated by IFN-gamma in experimental biliary atresia. J Clin Invest. 2004; 114:322–329. [PubMed: 15286798]
14. Shivakumar P, Sabla GE, Whitington P, et al. Neonatal NK cells target the mouse duct epithelium via Nkg2d and drive tissue-specific injury in experimental biliary atresia. J Clin Invest. 2009; 119:2281–2290. [PubMed: 19662681]
15. Lages CS, Simmons J, Chougnet CA, et al. Regulatory T cells control the CD8 adaptive immune response at the time of ductal obstruction in experimental biliary atresia. Hepatology. 2012; 56:219–227. [PubMed: 22334397]
16. Lages CS, Simmons J, Maddox A, et al. The dendritic cell-T helper 17-macrophage axis controls cholangiocyte injury and disease progression in murine and human biliary atresia. Hepatology. 2017; 65:174–188. [PubMed: 27641439]
17. Miethke AG, Zhang W, Simmons J, et al. Pharmacological inhibition of apical sodium-dependent bile acid transporter changes bile composition and blocks progression of sclerosing cholangitis in multidrug resistance 2 knockout mice. Hepatology. 2016; 63:512–523. [PubMed: 26172874]
18. Chen J, Bardes EE, Aronow BJ, et al. ToppGene Suite for gene list enrichment analysis and candidate gene prioritization. Nucleic Acids Res. 2009; 37:W305–311. [PubMed: 19465376]
19. Li Z, Agellon LB, Allen TM, et al. The ratio of phosphatidylcholine to phosphatidylethanolamine influences membrane integrity and steatohepatitis. Cell Metab. 2006; 3:321–331. [PubMed: 16679290]
20. Li J, Bessho K, Shivakumar P, et al. Th2 signals induce epithelial injury in mice and are compatible with the biliary atresia phenotype. J Clin Invest. 2011; 121:4244–4256. [PubMed: 22005305]
21. Moyer K, Kaimal V, Pacheco C, et al. Staging of biliary atresia at diagnosis by molecular profiling of the liver. Genome Med. 2010; 2:33. [PubMed: 20465800]
22. Moustafa T, Fickert P, Magnes C, et al. Alterations in lipid metabolism mediate inflammation, fibrosis, and proliferation in a mouse model of chronic cholestatic liver injury. Gastroenterology. 2012; 142:140–151 e112. [PubMed: 22001865]
23. Hardikar W, Ananthanarayanan M, Suchy FJ. Differential ontogenic regulation of basolateral and canalicular bile acid transport proteins in rat liver. J Biol Chem. 1995; 270:20841–20846. [PubMed: 7657669]
24. Cui YJ, Cheng X, Weaver YM, et al. Tissue distribution, gender-divergent expression, ontogeny, and chemical induction of multidrug resistance transporter genes (Mdr1a, Mdr1b, Mdr2) in mice. Drug Metab Dispos. 2009; 37:203–210. [PubMed: 18854377]
25. Li ZZ, Berk M, McIntyre TM, et al. Hepatic lipid partitioning and liver damage in nonalcoholic fatty liver disease: role of stearoyl-CoA desaturase. J Biol Chem. 2009; 284:5637–5644. [PubMed: 19119140]
26. Devaux PF. Static and dynamic lipid asymmetry in cell membranes. Biochemistry. 1991; 30:1163–1173. [PubMed: 1991095]
27. Walkey CJ, Yu L, Agellon LB, et al. Biochemical and evolutionary significance of phospholipid methylation. J Biol Chem. 1998; 273:27043–27046. [PubMed: 9765216]
28. Ling J, Chaba T, Zhu LF, Jacobs RL, Vance DE. Hepatic ratio of phosphatidylcholine to phosphatidylethanolamine predicts survival after partial hepatectomy in mice. Hepatology. 2012; 55:1094–1102. [PubMed: 22095799]
29. Ikenaga N, Liu SB, Sverdlov DY, Yoshida S, et al. A new Mdr2(−/−) mouse model of sclerosing cholangitis with rapid fibrosis progression, early-onset portal hypertension, and liver cancer. Am J Pathol. 2015; 185:325–334. [PubMed: 25478810]
30. Sontag TJ, Chellan B, Getz GS, Reardon CA. Differing rates of cholesterol absorption among inbred mouse strains yield differing levels of HDL-cholesterol. J Lipid Res. 2013; 54:2515–2524. [PubMed: 23812556]
31. Trivedi PJ, Weston CJ, Webb GJ, Newsome PN, et al. Serum alkaline phosphatase in multidrug resistance 2 (Mdr2(−/−)) knockout mice is strain specific. Hepatology. 2016; 63:346.

32. Krones E, Erwa W, Trauner M, Fickert P. Serum alkaline phosphatase levels accurately reflect cholestasis in mice. Hepatology. 2015; 62:981–983. [PubMed: 25424394]
33. Yan JJ, Jung JS, Lee JE, Lee J, et al. Therapeutic effects of lysophosphatidylcholine in experimental sepsis. Nat Med. 2004; 10:161–167. [PubMed: 14716308]
34. Sakata-Kaneko S, Wakatsuki Y, Usui T, et al. Lysophosphatidylcholine upregulates CD40 ligand expression in newly activated human CD4+ T cells. FEBS Lett. 1998; 433:161–165. [PubMed: 9738953]
35. Coutant F, Perrin-Cocon L, Agaugue S, et al. Mature dendritic cell generation promoted by lysophosphatidylcholine. J Immunol. 2002; 169:1688–1695. [PubMed: 12165488]
36. Asai A, Miethke A, Bezerra JA. Pathogenesis of biliary atresia: defining biology to understand clinical phenotypes. Nat Rev Gastroenterol Hepatol. 2015; 12:342–352. [PubMed: 26008129]
37. Shivakumar P, Sabla G, Mohanty S, et al. Effector role of neonatal hepatic CD8+ lymphocytes in epithelial injury and autoimmunity in experimental biliary atresia. Gastroenterology. 2007; 133:268–277. [PubMed: 17631148]
38. Mezina A, Gandhi K, Sabo A, et al. Abstract: Whole Exome Sequencing Identifies ABCB4 Gene Variants As Modifiers of Biliary Atresia Outcomes. Gastroenterology. 2014; 146:S-928.
39. Chianale J, Vollrath V, Wielandt AM, et al. Fibrates induce mdr2 gene expression and biliary phospholipid secretion in the mouse. Biochem J. 1996; 314(Pt 3):781–786. [PubMed: 8615769]

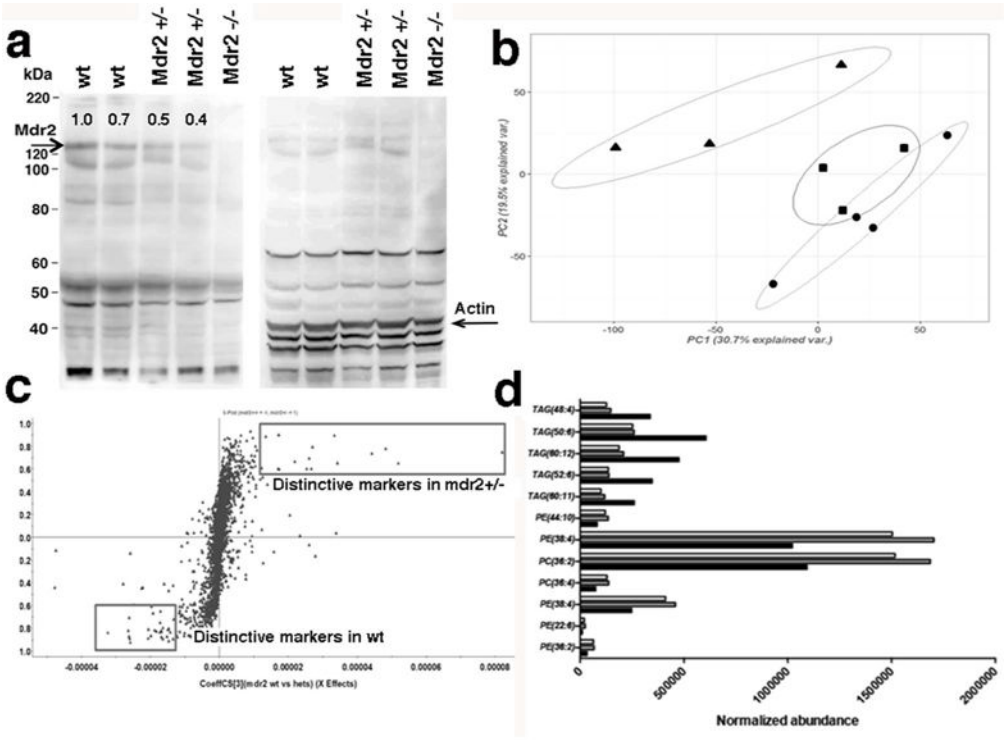

Figure 1.

Liver lipidomic patterns distinctly differ between neonatal wild type (wt) and Mdr2$^{+/-}$ mice. Protein blot analysis by SDS-PAGE was performed of crude hepatic protein extracts from neonatal mice. Numbers on blot in the left panel denote relative densitometry values for the intensity of the Mdr2-band at 140kDa normalized against the specific band recognized by the anti-Actin antibody at 43kDa in the right panel **(a)**. Principal component analysis (PCA) of total 7281 features (4502 negative compound ions, 2779 positive compound ions) detected by mass spectrometry (MS) on liver tissue homogenates from neonatal *Mdr2*$^{-/-}$ mice (denoted as circles), *Mdr2*$^{+/-}$ (squares) and wt mice (triangles) following exhaustive lipid extraction; MS analysis was performed in triplicate for each sample and the intensity of each compound ion is reported as average of three injections (**b).** S-plot comparing *Mdr2*$^{+/-}$ (right upper quadrant) with wt (left lower quadrant) with each point representing one of the 2779 positive compound ions. Compounds farthest away from Y-axis correspond to significantly changed metabolites in each group **(c).** Quantification of lipid species from metabolomic analysis shows that phosphatidylcholines (PC) and phosphatidylethanolamines (PE) accumulate while several triglyceride (TAG) species are reduced in livers of *Mdr2*$^{+/-}$ (gray fill columns) and *Mdr2*$^{-/-}$ (no fill columns) compared with wt mice (black fill columns) in **(d).**

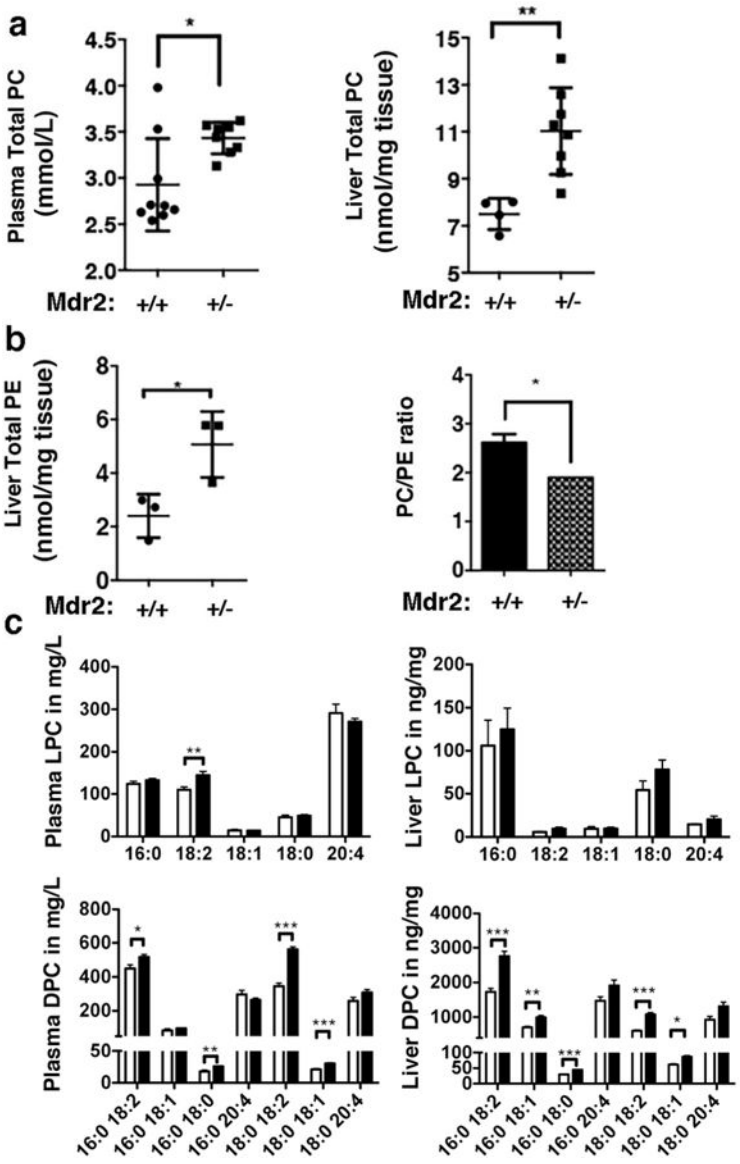

Figure 2.

Neonatal *Mdr2*$^{+/-}$ mice accumulate total and individual phosphatidylcholine (PC) and –ethanolamine (PE) species. Phospholipids were extracted from liver homogenates and plasma of 10-day-old mice of *Mdr2*$^{+/-}$ and wt mice and subjected to targeted mass spectrometry measurement for PC (**a**), for PE **(b)** and for individual lyso- and diacylphosphatidylcholines (LPC/DPC) (**c**). Black fill columns denote *Mdr2*$^{+/-}$ mice (n=8) and no fill columns denote wt mice (n=9). Unpaired T test was applied to test for statistically significant differences between groups with *p<0.05, **p<0.01, and ***p<0.005. Each dot in (**a**) and (**b**) represents a value from an individual animal.

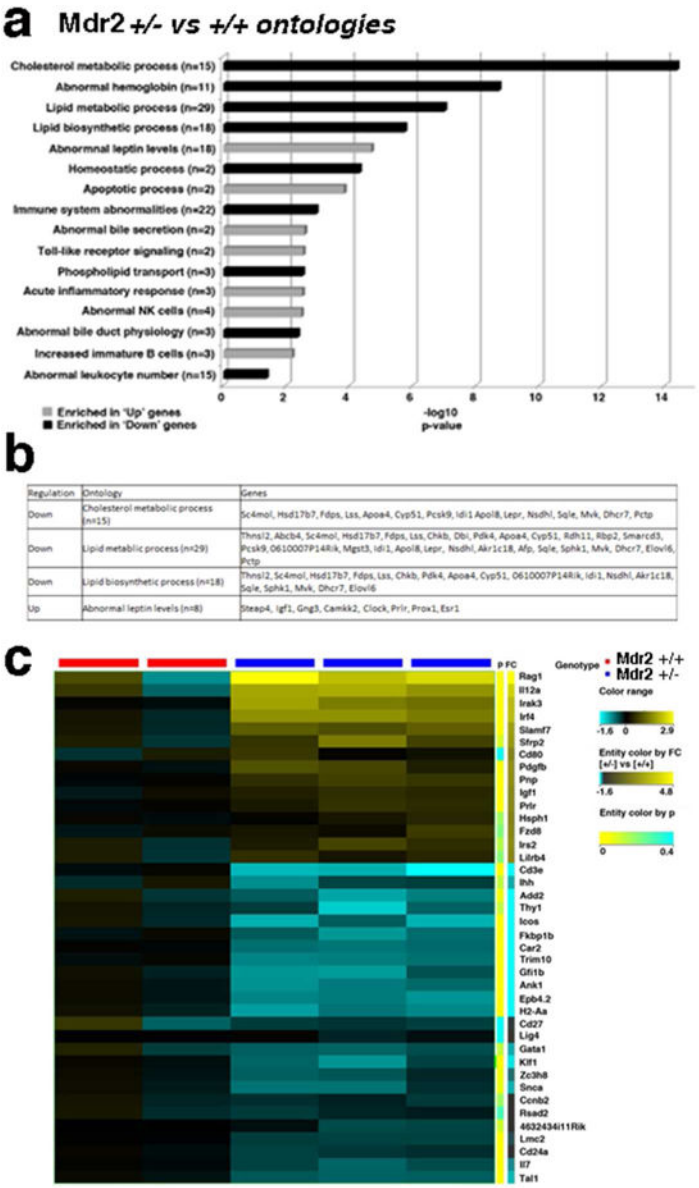

Figure 3.

Global transcriptomic profiles in livers of neonatal *Mdr2*$^{+/-}$ and wt mice. RNAseq studies were performed on total hepatic RNA from 10-day-old *Mdr2*$^{+/-}$ and *Mdr2*$^{+/+}$ mice. Based on pathway enrichment analysis, 16 pathways comprising significantly up- or downregulated genes in *Mdr2*$^{+/-}$ compared with *Mdr2*$^{+/+}$ control mice are depicted with p values for these pathways plotted as $-\log_{10}$ **(a).** Differentially expressed genes regulating lipid metabolisms are listed in (**b**). 40 genes from pathways relevant for immune function are displayed in the heatmap with expression levels normalized to control *Mdr2*$^{+/+}$ mice (**c).**

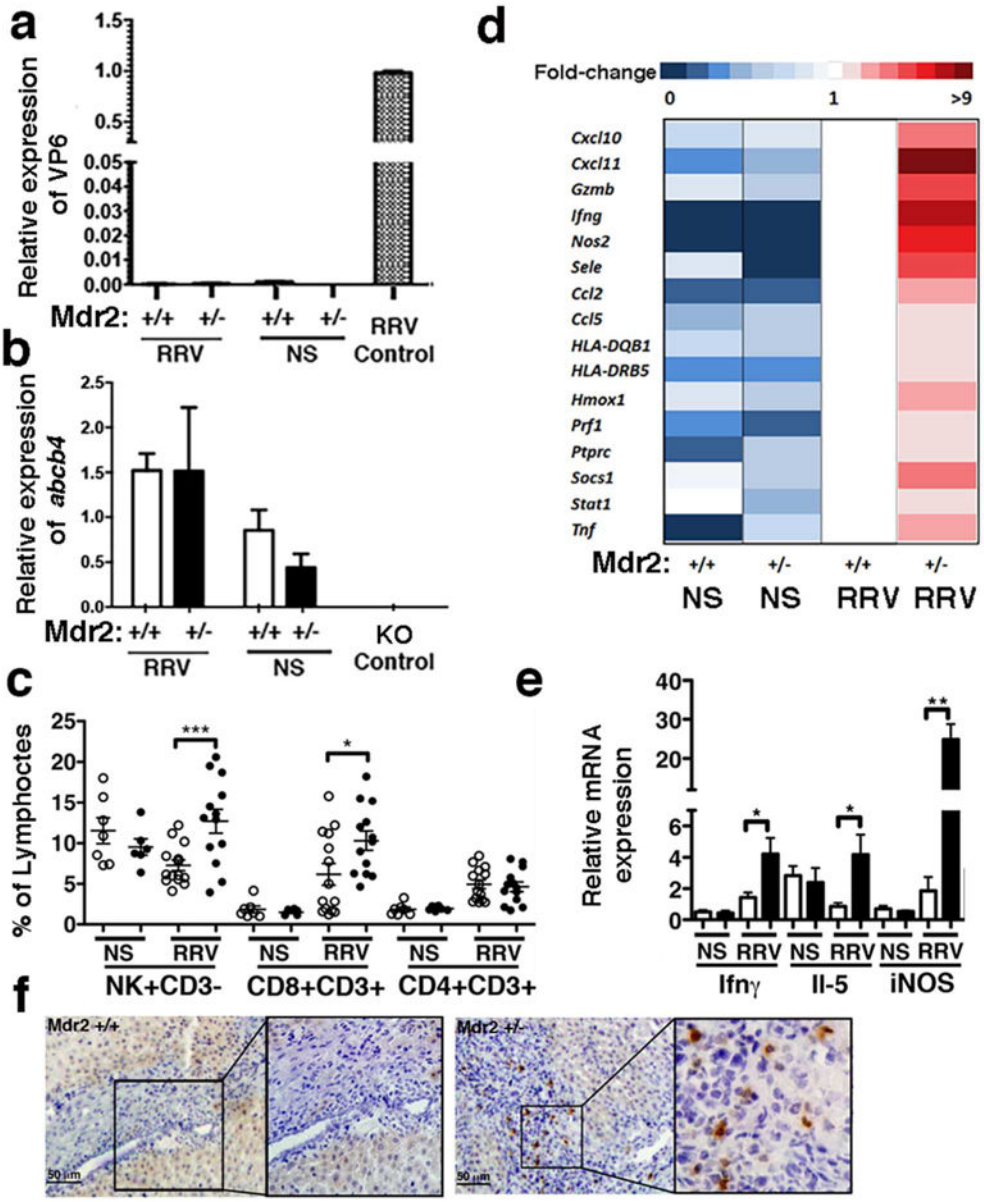

Figure 4.

Hepatic pro-inflammatory gene expression and effector lymphocyte recruitment following postnatal viral challenge of wt and *Mdr2*$^{+/-}$ mice. Livers were harvested on DOL10 following post-natal administration of RRV or NS. Hepatic expression of RRV-specific VP6 in *Mdr2*$^{+/-}$ and *Mdr2*$^{+/+}$ mice (n=3/group) was quantitated by SYBR green qPCR and compared to expression levels in infected cholangiocytes serving as positive control (**a**). Regulation of *Abcb4* mRNA expression following RRV infection was determined by TaqMan qPCR, with hepatic mRNA from an *Mdr2*$^{-/-}$ mouse serving as negative control (**b**). Hepatic mononuclear cells were subjected to flow cytometry and specific lymphocyte frequencies were determined within the size-gated lymphocyte population. Every dot represents % lymphocytes in an individual animal. No fill circles denote wt, black filled circles *Mdr2*$^{+/-}$ mice (**c**). Multiplex qPCR for 88 cytokines and chemokines was performed

using TaqMan Mouse Immune Arrays. The heatmap shows genes with >2-fold up-regulation in RRV-infected *Mdr2*$^{+/-}$ vs wt mice (**d**). Candidate gene expression studies on hepatic RNA were performed using SYBR green qPCR. No fill columns denote wt, black fill columns represent *Mdr2*$^{+/-}$ mice with n=6 animals/group (**e**). Protein expression of iNOS was detected by immunohistochemistry **(f)**. Unpaired t test was applied to test for statistical differences between groups in **c** and **e**, with *p<0.05, **p<0.01, and ***p<0.005.

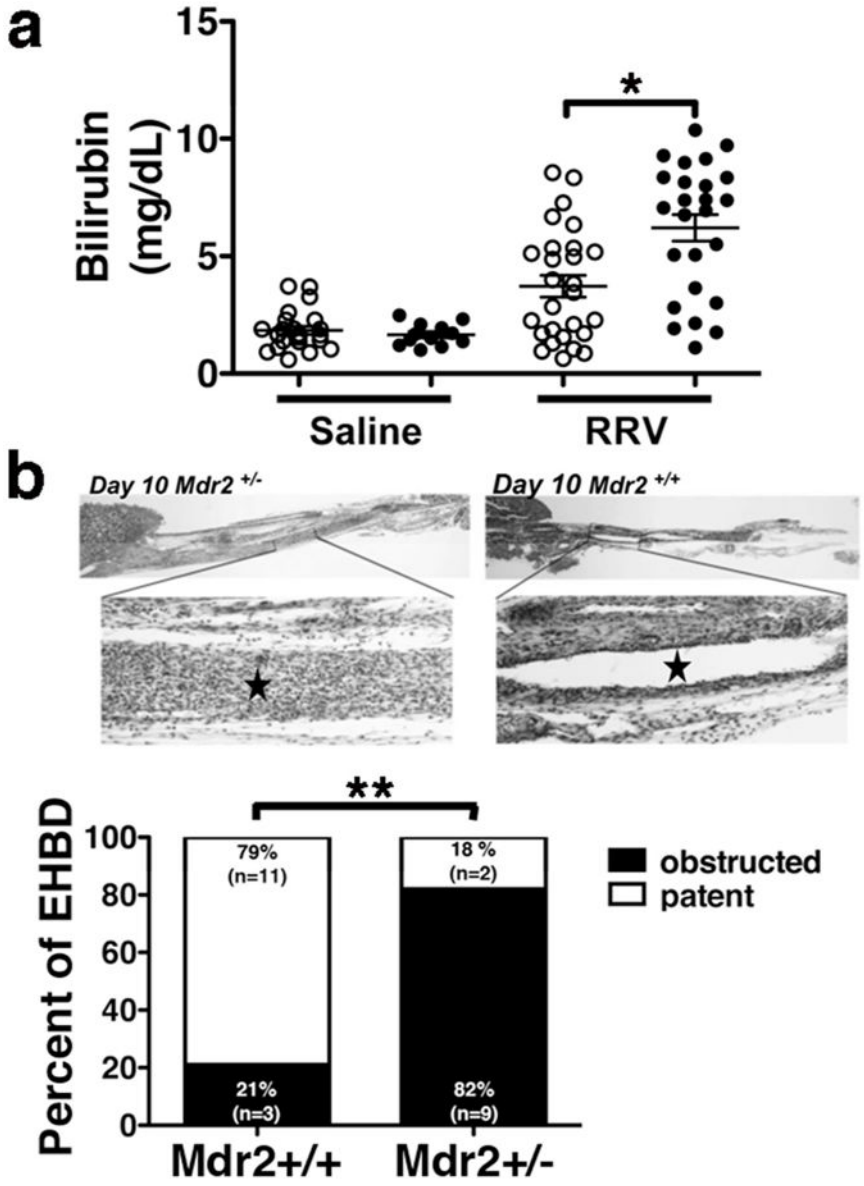

Figure 5.

Reduced Mdr2 expression predisposes to extrahepatic bile duct obstruction following RRV challenge. Total bilirubin was measured by colorimetric analysis from plasma obtained from neonatal *Mdr2*$^{+/+}$ (denoted by no fill circles) and *Mdr2*$^{+/-}$ mice (black fill circles) 8 days after either low-dose RRV or normal saline i.p. injection on DOL2 **(a).** Bile ducts were microdissected on day 8 p RRV, and H&E stained longitudinal consecutive sections were examined for patency or obstruction. Representative photomicrographs from bile ducts of both groups of mice with * denoting the bile duct lumen are shown in **b**. Unpaired t and Fisher exact tests were applied to test for statistical differences between groups in **a** and **b**, respectively, with *$p<0.05$, **$p<0.01$.

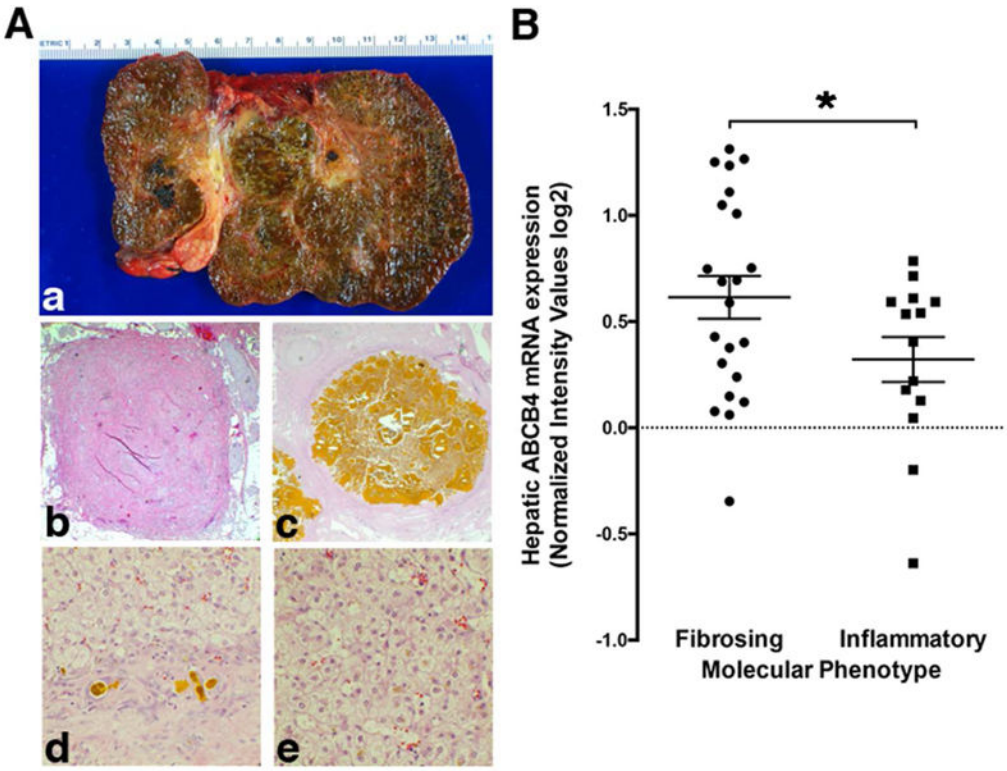

Figure 6.

Association between hepatic expression of *ABCB4* mRNA and inflammatory molecular signature in infants with EHBA. (**Aa**), Explanted liver of a 23-month-old-Somalian female with the clinical diagnosis of MDR3 disease, supported by bi-allelic non-synonymous variants in *ABCB4*. The explant shows biliary cirrhosis as well as (**Ab**) complete fibrous obliteration of the extrahepatic bile duct, (**Ad**) bile duct proliferation with bile plugs, **(Ac)** intrahepatic gallstones, and (**Ae**) canalicular cholestasis. Decreased hepatic expression of *ABCB4* in subjects with a transcriptomic profile of inflammatory EHBA is shown in **(B)**. Hepatic microarray gene expression data from a study on 40 subjects with EHBA identifying molecular signatures for inflammatory and fibrosing phenotypes were mined for the relative expression levels of *ABCB4*. Unpaired t test was applied to test for statistical differences between the groups with *$p<0.05$.